Nano Express

PAPER • **OPEN ACCESS**

Plasma treatment of MoS_2 field-effect transistors using solid-state fluorine source

To cite this article: Hiroki Kii *et al* 2025 *Nano Ex.* **6** 025008

NANO EXPRESS

PAPER

Plasma treatment of MoS_2 field-effect transistors using solid-state fluorine source

Hiroki Kii[1], **Naoka Nagamura**[2,3,4] **and Ryo Nouchi**[1,5]

[1] Department of Physics and Electronics, Osaka Prefecture University, Sakai 599-8570, Japan
[2] Research Center for Advanced Measurement and Characterization, National Institute for Materials Science, 3-13, Sakura, Tsukuba, Ibaraki 305-0003, Japan
[3] Faculty of Advanced Engineering, Tokyo University of Science, 6-3-1, Niijuku, Katsushika, Tokyo, 125-8585, Japan
[4] Research Institute of Electrical Communication, Tohoku University, 2-1-1 Katahira, Aobaku, Sendai 980-8577, Japan
[5] Department of Physics and Electronics, Osaka Metropolitan University, Sakai 599-8570, Japan

E-mail: r-nouchi@omu.ac.jp

OPEN ACCESS

RECEIVED
31 December 2024

REVISED
8 May 2025

ACCEPTED FOR PUBLICATION
20 May 2025

PUBLISHED
28 May 2025

Keywords: transition-metal dichalcogenide, surface passivation, hysteresis, water repellency, substitutional doping

Supplementary material for this article is available online

Abstract

Plasma treatment using a solid-state fluorine (F) source can mitigate the emission of F-containing gases into the environment. In this study, we investigated the processability of Ar-plasma-mediated F treatment using a polytetrafluoroethylene (PTFE) sheet as the F source. Surface treatment of two-dimensional (2D) semiconductor devices using this method resulted in an improvement in field-effect mobility and a reduction in hysteretic behavior. The prolonged treatment led to heavy p-doping, possibly owing to substitutional F doping. The treatment strength was controllable by the treatment time and sample position during the treatment. Placing the samples upstream resulted in a milder treatment compared to that positioned downstream. The controllability of the proposed method enables us to fine-tune the properties of devices based on 2D materials. The treatment elements could be controlled using sheets made of materials other than PTFE, indicating the broad applicability of this method.

1. Introduction

Two-dimensional (2D) semiconductors are promising candidates for post-silicon electronics because of their atomically thin nature, which enables the realization of ultrascaled field-effect transistors (FETs) [1]. The entire bodies of such ultrathin materials can be altered by modifying their surfaces. Plasma exposure is widely used to control the electronic properties of 2D semiconductors [2]. Oxygen-containing plasma improves photodetector performance [3, 4] and field-effect mobilities in FETs [5–7] via surface oxide formation [8] and defect passivation [9]. Argon- and nitrogen-containing plasmas have been used to improve the electrocatalytic activity [10–13] and supercapacitor performance [14] through defect formation and nitrogen doping [15].

Another important class of plasma gases in the semiconductor industry is those containing fluorine (F). F-containing plasmas have also been used to etch 2D materials [16–18], similar to their application in etching silicon-based materials. In addition to its use in etching processes, F-containing plasma has been confirmed to apply to surface modifications such as fluorination [18–20] and F-atom doping [21]. However, F-containing gases generally exhibit significantly higher global warming potential (GWP) values than that of CO_2. For example, GWP values for a 100-year time horizon were reported to be 7380, 9290, 10200, 12400, 14600, 17400, and 24300 for CF_4, C_3F_8, cyclic C_4F_8, C_2F_6, CHF_3, NF_3, and SF_6, respectively (1 for CO_2) [22]. Therefore, the emission of F-containing gases into the environment should be minimized. However, the degree of ionization in low-pressure plasma, commonly employed for surface modification and etching processes, is typically less than a few percent [23], and most of the inlet gas is exhausted from the process chamber as it is unionized. Although downstream abatement equipment has been developed in the semiconductor industry, the net destruction efficiency of these systems cannot achieve 100% owing to the byproducts generated during the treatment of

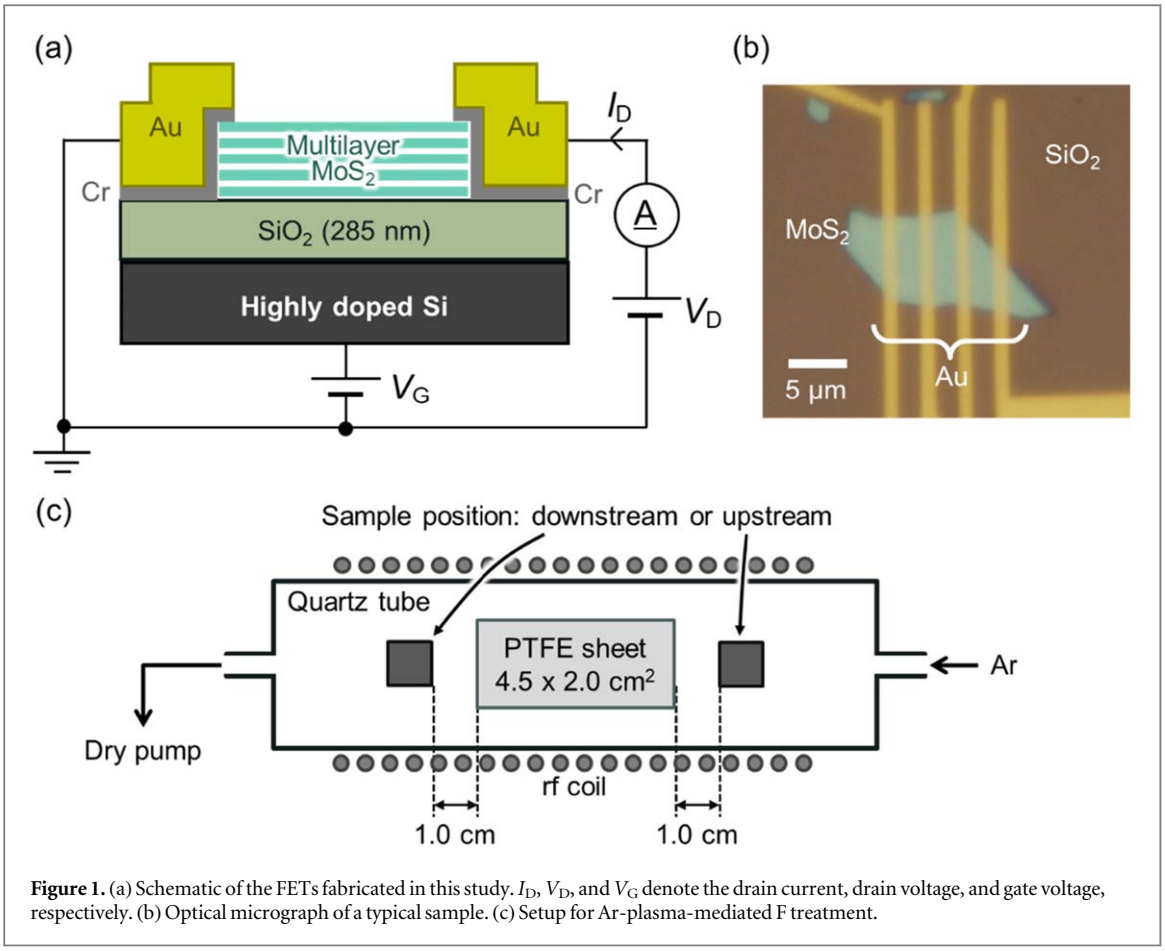

Figure 1. (a) Schematic of the FETs fabricated in this study. I_D, V_D, and V_G denote the drain current, drain voltage, and gate voltage, respectively. (b) Optical micrograph of a typical sample. (c) Setup for Ar-plasma-mediated F treatment.

F-containing gases [24]. In addition, destroying stable F-containing species such as CF_4 requires high-temperature processing, resulting in high energy consumption [25, 26].

In this study, a solid-state F source was employed for the surface modification of molybdenum disulfide (MoS_2), a representative 2D semiconductor. For a solid source, the unionized species remain inside the solid, which is expected to mitigate exhaust gas problems. An x-ray photoelectron spectroscopy study on argon plasma treatment of polytetrafluoroethylene (PTFE) [27] showed that the F/C ratio of the PTFE surface reduced from 2.0 to 1.4 by the treatment. This defluorination indicates the generation of reactive F species by breaking C—F bonds [28, 29]. In this study, we performed the F treatment of MoS_2 FETs using F species produced by the argon plasma treatment of a PTFE sheet. The strength of the F treatment can be controlled by the treatment time and position of the sample relative to that of the PTFE sheet. Although harsh treatment by placing the sample downstream resulted in heavy p-doping, as expected from the high electronegativity of F, milder treatment at the upstream position significantly improved the field-effect mobility. This study provides a facile method for tunable surface modification using F species by changing their position relative to the PTFE sheet.

2. Experimental

Highly doped Si wafers with a 285 nm thick thermal oxide layer were used as substrates for device fabrication. The substrate surface was cleaned by ultrasonication with acetone and 2-propanol and treated with an oxygen plasma cleaner (PDC-32G, Harrick Plasma). The MoS_2 flakes were transferred to a cleaned substrate by mechanical exfoliation of a natural crystal (SPI Supplies). Specifically, thick flakes were exfoliated from the source MoS_2 crystal using an adhesive tape. The flakes were thinned by repeated exfoliation using another tape. The thinned flakes on the tape were transferred to a dimethylpolysiloxane (PDMS) sheet (Gel-Pak PF-20/17-X4) by attaching the tape surface to the sheet and pressing it with the fingers. The PDMS sheet with thin flakes was then fixed on a glass slide. The flakes on the PDMS sheet were finally transferred to the SiO_2/Si substrate by attaching the surface of the PDMS sheet to the substrate and pressing it with the fingers. Au electrodes with Cr adhesion layers were fabricated on the transferred flakes by electron-beam lithography. Figures 1(a) and (b) show a schematic and optical micrograph of the fabricated FETs, respectively.

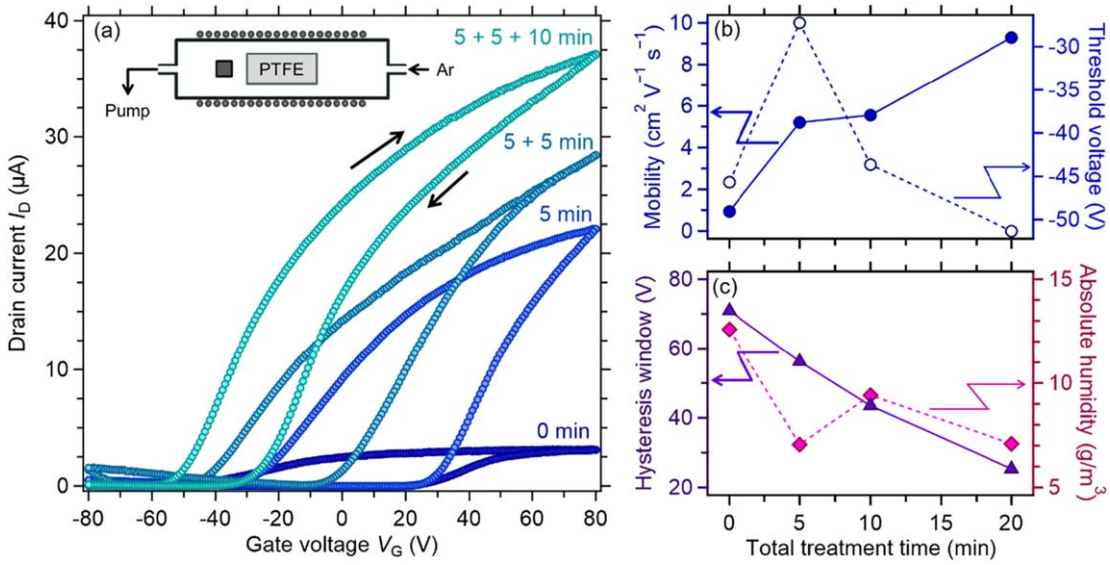

Figure 2. Effect of repeated treatments on the transfer characteristics of MoS_2 FETs placed downstream. The drain voltage, V_D, was set to 0.7 V. (a) Transfer characteristics measured before the series of treatments and after each treatment period. The arrows indicate the sweep direction of the gate voltage. Changes in (b) field-effect mobility, threshold voltage, and (c) hysteresis window. The threshold voltage difference between the forward and backward sweeps of the gate voltage defines the hysteresis window. The absolute humidity of the measurement environment is also shown in (c). See Figures S1(a) and S1(b) in the supplementary material for semi-logarithmic transfer characteristics and output characteristics, respectively.

The electrical characteristics of the FETs were measured using a semiconductor device analyzer (B1500A, Keysight) under ambient air in the dark. The FETs underwent Ar-plasma-mediated F treatment using a PTFE sheet. As shown in figure 1(c), the sample was placed downstream or upstream at a distance of 1.0 cm from a 1-mm-thick PTFE sheet (TOMBO™ No. 9000, Nichias, used after being cut into the dimensions of 4.5 cm × 2.0 cm) placed in the quartz tube of a plasma apparatus (PDC-32G, Harrick Plasma, operated with the rf power of 18 W). The typical base pressure of the system was 15 Pa. Ar was introduced when the pressure reached approximately 40 Pa.

The surface morphology of the MoS_2 FETs was acquired using an atomic force microscope (AFM; AFM5200S, Hitachi High-Tech) in the dynamic force mode. Chemical bonding states of MoS_2 flakes were investigated by x-ray photoemission spectroscopy (XPS) using a scanning photoelectron microscopy (SPEM) equipped at BL07LSU of SPring-8 [30, 31]. The excitation photon energy was set to 1000 eV. The incident x-rays were focused down to ~100 nm. The energy resolution was set at ~200 meV. The measurements were performed at room temperature. The Au 4f7/2 core-level peak at 84.0 eV from the gold film deposited close to the MoS_2 flakes was used for the binding energy scale calibrations.

3. Results and discussion

Figure 2(a) shows the transfer characteristics of the MoS_2 FETs before and after Ar-plasma-mediated F treatment. The treatment was repeated thrice for 5, 5, and 10 min (20 min in total). The transfer characteristics were measured before and after each treatment period. Field-effect mobilities (μ) and threshold voltages (V_{th}) were extracted using the following equation,

$$I_D = \frac{W}{L}\mu C_{ox}(V_G - V_{th})V_D$$

where W and L are the channel width and length, respectively; C_{ox} is the gate capacitance per unit area and equals 12.1 nF cm^{-2} for the 285-nm-thick SiO_2 layer. Least-squares fitting of the transfer curves within the 20-V range around the gate voltage corresponding to the maximum transconductance (dI_D/dV_G) yielded the values shown in figure 2(b). The μ values are limited by the electrode contacts as explained below. The thicknesses of the flakes used in this study were greater than 10 nm (see the supplementary material). The source and drain electrodes were fabricated as the top contacts. Thus, charge carriers were injected mainly from the top surface of the thick MoS_2 flakes. On the other hand, the gate stack was fabricated as a global back gate. Thus, transistor channels were formed at the bottom surface of the flakes. Therefore, the devices in the present study suffered from a large

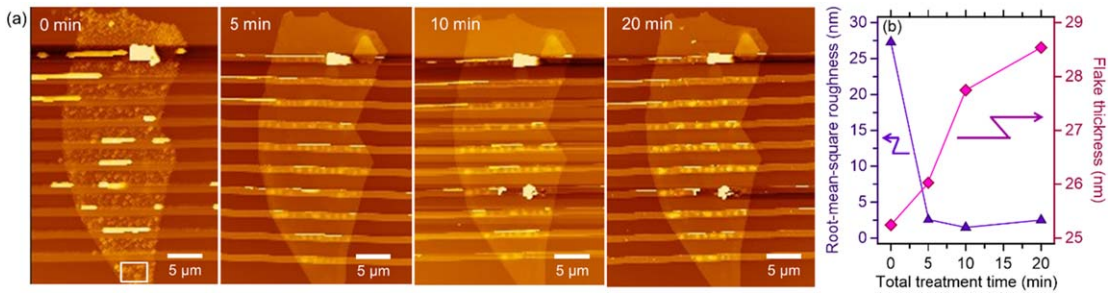

Figure 3. Effect of repeated treatments on the surface morphology of MoS_2 FETs placed downstream. (a) AFM images before the series of treatments and after each treatment. (b) Root mean square roughness of area indicated by the white rectangle in (a) and flake thickness.

access resistance from the top to the bottom surface of the flakes. In addition, the contact metal used in this study, Au (with an adhesion layer of Cr), is not a good electron injector, considering its work function.

As the total treatment time was prolonged, μ improved, as evidenced by the increased current. In addition, hysteretic behavior was significantly suppressed. As shown in figure 2(c), the hysteresis window, defined as the difference in the threshold voltage between the forward and backward sweeps, was reduced from 71 to 25 V after a series of treatment processes. The hysteretic behavior of MoS_2 FETs is attributed to the presence of water [32–34]. A smaller hysteresis with a longer treatment time indicates fewer water molecules near the FET channel. The hysteresis window shows a stronger correlation with the treatment time than with the absolute humidity, which suggests that the plasma treatment has a stronger impact on the device characteristics. The possible acquisition of the water-repellent property is likely attributable to F passivation of the MoS_2 flakes by the treatment. Water molecules possess an electric dipole that induces potential fluctuations and leads to charge-carrier scattering. Therefore, the improved mobility can be attributed to the possible acquisition of water-repellent properties of F treatment.

The effect of the F treatment on the surface morphology was investigated by AFM. Figure 3(a) shows a series of AFM images acquired before starting the treatment and after each treatment. Before starting the treatment, the surfaces of the MoS_2 flakes were covered by particles, which could have originated from the exfoliation and lithography processes. The particles were removed mainly after the initial treatment. As shown in figure 3(b), this was evidenced by an initial decrease in the root-mean-square roughness of the MoS_2 flake surface. It is well known that surface scattering of carriers is significant for carrier transport in thin films [35, 36]. The presence of surface adsorbates transforms the specular reflectance of carriers at the film surface into diffusive scattering, increasing the electrical resistance. Such adsorbates include gas molecules [37], chemisorbed species [38, 39], and large molecules [40]. Process residues on the MoS_2 surface can also act as scattering centers. Therefore, the improved mobility due to F treatment is partially attributable to removing process residues.

However, plasma treatments for 5 min without the PTFE sheet were found to degrade the electrical properties (see figure S2 in the supplementary material). The device was placed in a position surrounded by an rf coil. Therefore, the device was subjected to direct exposure to high-energy plasma species, which damaged the device. On the other hand, figure 2(a) shows that plasma treatment with a PTFE sheet for 5 min enhanced electrical properties. Resist residues should also be removed by treatment without PTFE sheets. Therefore, mechanisms other than resist-residue removal should be the leading cause of the improvement by treatment with PTFE sheets. One possible mechanism is the passivation effect of the fluorocarbon species originating from the PTFE sheet. Fluorocarbon films are known to be deposited by CF_4-gas plasma treatments [41]. A similar phenomenon was expected in the case of the solid-state F source. As shown in figure 2(c), an increase in flake thickness after repeated treatments was confirmed by AFM observations. After forming a thin film of CF-related species, the CF_x layer covering the MoS_2 surface may have prevented the direct impingement of high-energy plasma species. In addition, CF_x deposition can change the water repellency and dielectric environment of MoS_2 flakes. The former mitigates Coulomb scattering of charge carriers as explained above. For the latter, an increase in dielectric constant is known to reduce charged-impurity scattering of charge carriers in the channel, leading to an increase in mobility [42, 43]. The dielectric constant of PTFE has been reported to be around 2.0 [44]. The alteration of the dielectric on the top surface of the MoS_2 layer from air to a CF_x film increases the dielectric constant, thus increasing the mobility.

To confirm the introduction of F species by plasma treatment of MoS_2 flakes, pinpoint measurements were performed using synchrotron radiation micro-XPS with high spatial resolution, which allows selective analysis of microscale MoS_2 flakes. One MoS_2 flake was processed by plasma treatment for a short period (30 s at the

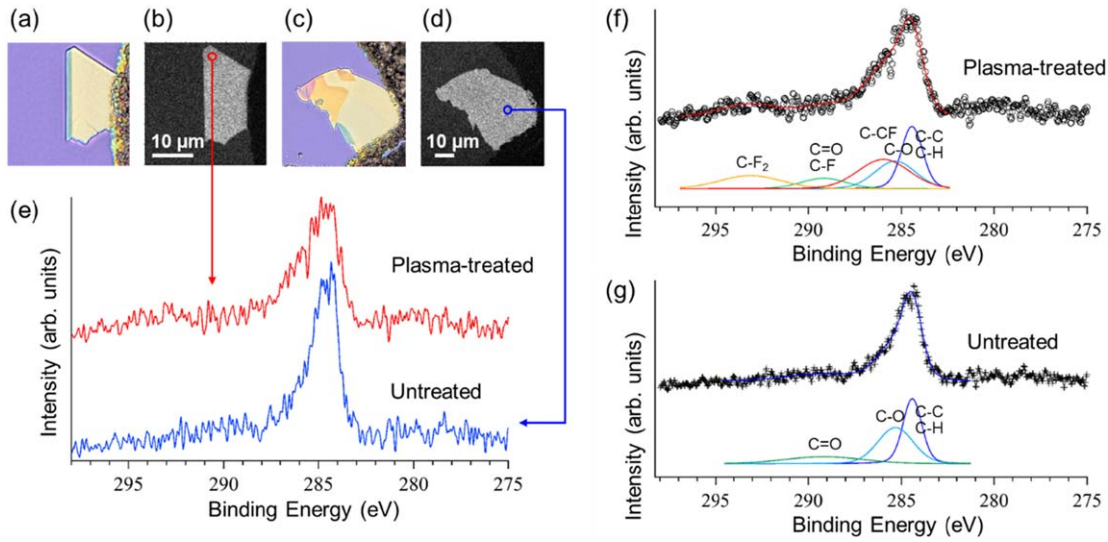

Figure 4. Micro-XPS analysis of plasma-treated and untreated MoS_2 flakes. (a) Optical microscopy and (b) spectral intensity mapping of Mo 3d obtained by SPEM for a plasma-treated MoS_2 flake. (c) Optical microscopy and (d) spectral intensity mapping of Mo 3d obtained by SPEM for an untreated MoS_2 flake. (e) Pinpoint C 1s core-level spectra at positions indicated in (b) and (d). (f) Results of peak deconvolution of the C 1s spectrum shown in the red curve of (e) measured on a plasma-treated MoS_2 flake. (g) Results of peak deconvolution of the C 1s spectrum shown in the blue curve of (e) measured on an untreated MoS_2 flake. See figure S3 in the supplementary material for Mo 3d and S 2s spectra.

downstream position) to prevent the deposition of a thick fluorocarbon film. Figure 4 shows the C 1s core-level spectra of plasma-treated and untreated MoS_2 flakes. The C peaks observed in the untreated sample were attributable to hydrocarbon contamination from air or residues from the adhesive tape used in the exfoliation process. As shown in figure 3, these C contaminations were largely removed by plasma treatment. The plasma treatment should have introduced fluorocarbon species originating from the PTFE source in addition to unremoved contamination. The plasma-treated sample showed an increase in the intensity of the high-energy side (~286 eV) of the C 1s main peak, which is attributable to the introduction of C-CF. In addition, a peak centered at ~293 eV was discernible only in the plasma-treated sample, originating from C-F_2. The observed differences in the C 1s peak shape in the pinpoint XPS spectra confirm the introduction of F-related species into the plasma-treated sample.

Ar-plasma-mediated F treatment was conducted under a medium vacuum (~40 Pa). Under these conditions, the gas in the process chamber exhibits a viscous flow. The F species generated from the PTFE sheet were transported downstream by the residual gas flow. Therefore, the sample position during treatment is expected to affect the strength of the treatment. Figures 5(a)–(d) and (e) show the changes in the transfer characteristics with treatment at the downstream and upstream positions, respectively. It should be noted that the current level of the device shown in figure 5(c) is higher than that of the other devices. This can be explained by the thinner flake used in the device (see figure S4 in the supplementary material), which results in the lowest access resistance between the top electrode contact and the bottom channel. As shown in figures 5(a)–(d), the characteristics after treatment at the downstream position gradually changed from n- to p-type conduction as the treatment time increased. The appearance of a p-type branch and positive shift in the threshold voltage of the n-type branch (see figures 5(b) and (c)) are clear signs of substitutional p-doping [21]. The strong electron-withdrawing ability of fluorine, due to its high electronegativity, leads to hole doping. Because the electronegativity of carbon is nearly the same as that of sulfur, substitutional p-doping by carbon is much weaker than that by fluorine [45]. The carbon-to-fluorine ratio of the PTFE sheet was 1:2. Therefore, the carrier-doping effect is most likely governed by the incorporation of F atoms. The changes in carrier concentration resulting from the plasma treatment were calculated based on the difference in the threshold voltage before and after treatment. The results of these calculations are presented in table 1. The carrier concentration resulting from the addition of F as a dopant was higher than 10^{13} cm^{-2} in the case with the highest dopant concentration. Although the total treatment time in figure 2 was the same as that shown in figure 5(c), the difference in the resultant transfer characteristics suggests the presence of an incubation time for substitutional doping, similar to what was observed in the etching of MoS_2 by CF_4 plasma [16]. If the treatment period is insufficient for doping, plasma-induced damage may be recovered during air exposure during electrical characterization. For the treatment at the upstream position, the change in the transfer characteristics was similar to that shown in figure 2. This result

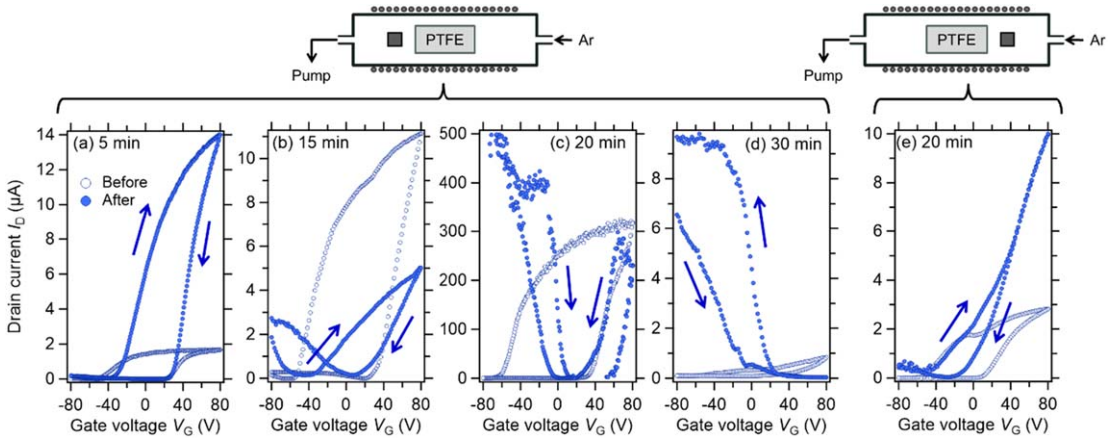

Figure 5. Effect of treatment time and sample position during treatment on the transfer characteristics of MoS_2 FETs. The samples were positioned (a)–(d) downstream and (e) upstream. The treatment time was indicated in each figure. The drain voltage V_D was set to 0.5 V. The data points before and after treatment are displayed as open and solid circles, respectively. The arrows indicate the sweep direction of the gate voltage. See figure S4 in the supplementary material for semi-logarithmic transfer characteristics, output characteristics, and AFM images.

Table 1. Changes in the carrier concentration, Δn, calculated from the difference in the n-channel threshold voltage before and after the treatment, ΔV_{th}, using the relationship $\Delta n = C_{ox}\Delta V_{th}/e$, where e is the elementary charge.

Figure No.	5 (a)	5 (b)	5 (c)	5 (d)	5 (e)
V_{th} (before) [V]	−49.2	−53.6	−59.8	−79.8	−54.0
V_{th} (after) [V]	−27.3	−34.3	61.3	>80	−51.5
ΔV_{th} [V]	21.9	19.3	121.1	>159.8	2.5
Δn [10^{12} cm^{-2}]	1.7	1.5	9.2	>12.1	0.2

indicates that the strength of the F treatment was reduced by positioning the sample upstream. Therefore, Ar-plasma-mediated F treatment can be controlled by controlling the position of the sample during treatment.

Thinner flakes should be affected more severely than thicker ones; for example, the ratio of a portion doped with F atoms to that remaining undoped is expected to be higher in thinner flakes. The sample positioned upstream (thickness: 23.2 nm; see figure S4 in the supplementary material) showed an increase in drain current after 20-min of treatment. The drain current increased with the gate voltage, indicating n-channel conduction. At the downstream position, another sample with a similar thickness (23.3 nm) was treated for 15 min. Even with a shorter treatment time, the treatment resulted in a reduction in n-channel conduction and the appearance of p-channel conduction. This is a clear indication of significant F doping. These results indicate that the sample position during treatment is a more dominant factor than flake thickness.

PTFE sheets are aggregates of TFE-based molecular chains. Therefore, plasma-induced damage to the PTFE surface should be considered at the molecular scale. A single chain can be easily removed from the surface by exposure to the plasma. After removing the chain, another fresh chain will soon appear on the underlying surface. Looking at a single site, the surface condition changes repeatedly. The stage of chain removal differs from position to position on the PTFE surface. Therefore, the surface condition can be regarded as constant on average during plasma exposure. As shown in figures 5(a)–(d), the present process possesses a certain controllability of the doping level by changing the treatment time. The monotonic dependence on the treatment time might support the constancy of the PTFE surface conditions.

The transfer characteristics shown in Figures S1 and S3 in the supplementary material show that the gate leakage current tends to increase after exposure to the fluorine plasma. The slight increase in the gate leakage may be attributed to the carbon components that are deposited in the CF_x layers during the plasma treatment. These CF_x films are deposited onto the entire substrate surface because the plasma treatment was conducted without a shadow mask. The finite conductivity of the amorphous carbon (a-C) parts embedded in the CF_x films may provide a gate leakage path when the a-C reaches the substrate edges and bypasses the gate insulator. The gate leakage problem is expected to be mitigated by the co-introduction of oxygen gas during the plasma treatment, which would serve to burn out the residual carbon by oxidation. In addition, a certain number of carbon atoms are expected to be incorporated into the MoS_2 lattice. The incorporation of carbon atoms might

cause deteriorative effects, such as degradation of the carrier mobility, which are also expected to be mitigated by the co-introduction of oxygen gas during the plasma treatment.

4. Conclusion

The Ar-plasma-mediated F treatment of MoS_2 FETs was conducted using a PTFE sheet as the solid-state F source. In this treatment, the unionized F species remained inside the solid, mitigating the emission of high-GWP F-based gases into the environment. Repeating the short-term treatment gradually improved the field-effect mobilities and reduced the hysteretic behavior of the transfer characteristics. The latter effect is attributed to the possible acquisition of water-repellent properties through F passivation, which reduces the potential fluctuation caused by the electric dipoles of the water molecules. Additionally, the treatment was confirmed to remove the fabrication process residues from the MoS_2 surface. The reduced number of water molecules and surface contaminants results in a reduction of the concentration of charge-carrier scattering centers, which leads to improved mobility. The strength of the treatment was controlled by the treatment time and position of the sample during the treatment. While the placement of samples at upstream positions led to a similar result with a shorter treatment time at downstream positions, the samples placed downstream were found to be heavily p-doped, possibly owing to substitutional F doping. This study elucidates the processability of F-based surface treatments using a solid-state F source. The device properties imparted by this treatment can be tuned by exploiting the controllability of this method. In principle, plasma-mediated treatment with a solid-state source can be applied to elements other than F by simply changing the solid-source material, which allows for altering surface properties without modifying the plasma gas species.

Acknowledgments

This study was supported by JSPS KAKENHI Grant Numbers JP19H02561, JP22H01912, JP23K23180, JP21H01638, JP21H04696, and JP24K01243; JST PRESTO Grant Numbers JPMJPR20T8, JPMJPR20T7, and JPMJPR17NB; and the Murata Science Foundation. The spectral datasets were obtained with the support of the University of Tokyo Outstation Beamline (BL07LSU) at SPring-8 (Proposal Numbers: 2021A7421, 2021A7422, 2021B7433, 2021B7435, 2022A7444). We thank Shun Konno (Tokyo University of Science) and Wenxiong Zhang (The University of Tokyo) for measurements in SPring-8.

Data availability statement

All data that support the findings of this study are included within the article (and any supplementary files).

ORCID iDs

Naoka Nagamura https://orcid.org/0000-0002-7697-8983
Ryo Nouchi https://orcid.org/0000-0002-7232-4827

References

[1] Zeng S, Liu C and Zhou P 2024 Transistor engineering based on 2D materials in the post-silicon era *Nat. Rev. Electr. Eng.* **1** 335–48
[2] Jadwiszczak J, Kelly D J, Guo J, Zhou Y and Zhang H 2021 Plasma treatment of ultrathin layered semiconductors for electronic device applications *ACS Appl. Electron. Mater.* **3** 1505–29
[3] Jadwiszczak J, Li G, Cullen C P, Wang J J, Maguire P, Duesberg G S, Lunney J G and Zhang H 2019 Photoresponsivity enhancement in monolayer MoS_2 by rapid O_2:Ar plasma treatment *Appl. Phys. Lett.* **114** 091103
[4] Wu J, Li S, Wang X, Huang Y, Huang Y, Chen H, Chen J, She J and Deng S 2023 Plasma treatment for achieving oxygen substitution in layered MoS_2 and the room-temperature mid-infrared (10 μm) photoresponse *ACS Appl. Mater. Interfaces* **15** 58556–65
[5] Dhall R, Li Z, Kosmowska E and Cronin S B 2016 Charge neutral MoS_2 field effect transistors through oxygen plasma treatment *J. Appl. Phys.* **120** 195702
[6] Jadwiszczak J *et al* 2018 Oxide-mediated recovery of field-effect mobility in plasma-treated MoS_2 *Sci. Adv.* **4** eaao5031
[7] Li Z, Liu L and Xu J-P 2021 Largely enhanced mobility of MoS_2 field-effect transistors by optimizing O_2-plasma treatment on MoS_2 *IEEE Trans. Electron Devices* **68** 4614–7
[8] Kang N, Paudel H P, Leuenberger M N, Tetard L and Khondaker S I 2014 Photoluminescence quenching in single-layer MoS_2 via oxygen plasma treatment *J. Phys. Chem. C* **118** 21258–63
[9] Nan H, Wu Z, Jiang J, Zafar A, You Y and Ni Z 2017 Improving the electrical performance of MoS_2 by mild oxygen plasma treatment *J. Phys. D: Appl. Phys.* **50** 154001
[10] Nguyen A D *et al* 2019 Nitrogen-plasma-treated continuous monolayer MoS_2 for improving hydrogen evolution reaction *ACS Omega* **4** 21509–15

[11] Wang J, Feng X, Hedman D, Wu X, Pan H and Zhang Q 2022 Enhancing the hydrogen evolution reaction on MoS_2 flakes by cold plasma treatment *Electrochem. Commun.* **137** 107250
[12] Huang Y-S, Liu Y-T, Perng T-P, Lu M-Y, Chueh Y-L and Chen L-J 2023 Enhancing photocatalytic properties of continuous few-layer MoS_2 thin films for hydrogen production by water splitting through defect engineering with Ar plasma treatment *Nano Energy* **109** 108295
[13] Li Y, Wan Y, Yao J, Zheng H, Wang X, Liu X, Ouyang B, Huang C, Deng K and Kan E 2023 Enhanced electrocatalytic hydrogen evolution from nitrogen plasma-tailored MoS_2 nanostructures *Phys. Chem. Chem. Phys.* **25** 31628–35
[14] Rui S, Li Z, Meng L, Wang Q, Xu J, Zhao Y, Jia Q, Li H, Lu S and Zhang Y 2025 Citric acid and plasma treated MoS_2 for high-performance supercapacitors *J. Mater. Chem. C* **13** 849–57
[15] Azcatl A *et al* 2016 Covalent nitrogen doping and compressive strain in MoS_2 by remote N_2 plasma exposure *Nano Lett.* **16** 5437–43
[16] Jeon M H, Ahn C, Kim H, Kim K N, LiN T Z, Qin H, Kim Y, Lee S, Kim T and Yeom G Y 2015 Controlled MoS_2 layer etching using CF_4 plasma *Nanotechnology* **26** 355706
[17] Ghasemi F, Abdollahi A and Mohajerzadeh S 2019 Controlled plasma thinning of bulk MoS_2 flakes for photodetector fabrication *ACS. Omega* **4** 19693–704
[18] Shin Y *et al* 2024 Facilitated fluorination and etching of 2D materials *Appl. Surf. Sci.* **645** 158857
[19] Bon S B, Valentini L, Verdejo R, Garcia Fierro J L, Peponi L, Lopez-Manchado M A and Kenny J M 2009 Plasma fluorination of chemically derived graphene sheets and subsequent modification with butylamine *Chem. Mater.* **21** 3433–8
[20] Zhang H, Fan L, Dong H, Zhang P, Nie K, Zhong J, Li Y, Guo J and Sun X 2016 Spectroscopic investigation of plasma-fluorinated monolayer graphene and application for gas sensing *ACS Appl. Mater. Interfaces* **8** 8652–61
[21] Chee S-S, Jang H, Lee K and Ham M-H 2020 Substitutional fluorine doping of large-area molybdenum disulfide monolayer films for flexible inverter device arrays *ACS Appl. Mater. Interfaces* **12** 31804–9
[22] Climate Change 2021: The Physical Science Basis 2021 Table 7.SM.7 Sixth Assessment Report of the Intergovernmental Panel on Climate Change (https://www.ipcc.ch/report/ar6/wg1/)
[23] Suzuki K, Okudaira S, Sakudo N and Kanomata I 1977 Microwave plasma etching *Jpn. J. Appl. Phys.* **16** 1979
[24] Ko D G, Ko S J, Choi E K, Min S G, Oh S H, Jung J, Kim B M and Im I-T 2014 Perfluorocarbon destruction and removal efficiency: considering the byproducts and energy consumption of an abatement system for microelectronics manufacturing *IEEE Trans. Semicond. Manuf.* **27** 456–61
[25] Iacopi F and McIntosh M 2019 Opportunities and perspectives for green chemistry in semiconductor technologies *Green Chem.* **21** 3250–5
[26] Chang M B and Chang J-S 2006 Abatement of PFCs from semiconductor manufacturing processes by nonthermal plasma technologies: a critical review *Ind. Eng. Chem. Res.* **45** 4101–9
[27] Kim S R 2000 Surface modification of poly(tetrafluoroethylene) film by chemical etching, plasma, and ion beam treatments *J. Appl. Polym. Sci.* **77** 1913–20
[28] Carbone E A D, Verhoeven M W G M, Keuning W, Mullen J J A M and van der 2016 PTFE treatment by remote atmospheric Ar/O_2 plasmas: a simple reaction scheme model proposal *J. Phys. Conf. Ser.* **715** 012011
[29] Perry C C, Wagner A J and Howard Fairbrother D 2002 Electron stimulated C–F bond breaking kinetics in fluorine-containing organic thin films *Chem. Phys.* **280** 111–8
[30] Horiba K, Nakamura Y, Nagamura N, Toyoda S, Kumigashira H, Oshima M, Amemiya K, Senba Y and Ohashi H 2011 Scanning photoelectron microscope for nanoscale three-dimensional spatial-resolved electron spectroscopy for chemical analysis *Rev. Sci. Instrum.* **82** 113701
[31] Nagamura N, Konno S, Matsumoto M, Zhang W, Kotsugi M, Oshima M and Nouchi R 2023 Photoelectron spectromicroscopy analysis of graphene during gate-controlled photo-oxidation process *Nano Express* **3** 044003
[32] Kim W, Javey A, Vermesh O, Wang Q, Li Y and Dai H 2003 Hysteresis caused by water molecules in carbon nanotube field-effect transistors *Nano Lett.* **3** 193–8
[33] Wang H, Wu Y, Cong C, Shang J and Yu T 2010 Hysteresis of electronic transport in graphene transistors *ACS. Nano* **4** 7221–8
[34] Late D J, Liu B, Matte H S S R, Dravid V P and Rao C N R 2012 Hysteresis in single-layer MoS_2 field effect transistors *ACS. Nano* **6** 5635–41
[35] Fuchs K 1938 The conductivity of thin metallic films according to the electron theory of metals *Math. Proc. Cambridge Philos. Soc.* **34** 100–8
[36] Sondheimer E H 1952 The mean free path of electrons in metals *Adv. Phys.* **1** 1–42
[37] Wissmann P 1972 The effect of gas adsorption on the conductivity of thin metal films *Thin Solid Films* **13** 189–93
[38] Yang F, Donavan K C, Kung S-C and Penner R M 2012 The surface scattering-based detection of hydrogen in air using a platinum nanowire *Nano Lett.* **12** 2924–30
[39] Ding M, He Q, Wang G, Cheng H-C, Huang Y and Duan X 2015 An on-chip electrical transport spectroscopy approach for *in situ* monitoring electrochemical interfaces *Nat. Commun.* **6** 7867
[40] Nouchi R and Kanno I 2005 Charge transfer and formation of conducting C_{60} monolayers at C_{60}/noble-metal interfaces *J. Appl. Phys.* **97** 103716
[41] Jin H, Fan F, Yuan Z and Li Y 2020 Investigation of the formation mechanism of the fluorocarbon film in CF_4 plasma processing of fused silica *Optik* **202** 163693
[42] Jang C, Adam S, Chen J-H, Williams E D, Das Sarma S and Fuhrer M S 2008 Tuning the effective fine structure constant in graphene: opposing effects of dielectric screening on short- and long-range potential scattering *Phys. Rev. Lett.* **101** 146805
[43] Radisavljevic B and Kis A 2013 Mobility engineering and a metal–insulator transition in monolayer MoS_2 *Nat. Mater.* **12** 815–20
[44] Wang L, Liu C, Shen S, Xu M and Liu X 2020 Low dielectric constant polymers for high speed communication network *Adv. Ind. Eng. Polym. Res.* **3** 138–48
[45] Yue Q, Chang S, Qin S and Li J 2013 Functionalization of monolayer MoS_2 by substitutional doping: a first-principles study *Phys. Lett. A* **377** 1362–7